Methimazole-Related Substances: Structural Characterization and In Silico Toxicity Assessment

Štefan, Leo; Đilović, Ivica; Saftić Martinović, Lara; Vianello, Robert; Čikoš, Ana

crystals

MDPI

Article

Methimazole-Related Substances: Structural Characterization and *In Silico* Toxicity Assessment

Leo Štefan [1], Ivica Đilović [2], Lara Saftić Martinović [3,4], Robert Vianello [5] and Ana Čikoš [6,*]

1 JGL d.d. Jadran Galenski Laboratorij, 51000 Rijeka, Croatia
2 Faculty of Science, Department of Chemistry, University of Zagreb, 10000 Zagreb, Croatia
3 Faculty of Biotechnology and Drug Development, University of Rijeka, 51000 Rijeka, Croatia; lara.saftic.martinovic@medri.uniri.hr
4 Medical Faculty, University of Rijeka, 51000 Rijeka, Croatia
5 Laboratory for the Computational Design and Synthesis of Functional Materials, Division of Organic Chemistry and Biochemistry, Ruđer Bošković Institute, 10000 Zagreb, Croatia; robert.vianello@irb.hr
6 NMR Centre, Ruđer Bošković Institute, 10000 Zagreb, Croatia
* Correspondence: ana.cikos@irb.hr

Abstract: The continuous tightening of pharmaceutical regulations forces drug manufacturers to unambiguously characterize the substances related to the active pharmaceutical ingredients (API). Here, we report the synthesis, complete spectroscopic, chromatographic, thermal and computational characterization, as well as *in silico* prediction of bacterial mutagenicity for two previously reported but never fully characterized impurities of methimazole. Additionally, their structures were analyzed by single-crystal X-ray diffraction. 1-Methyl-(2-methylthio)-1*H*-imidazole also known as methimazole impurity C, was obtained mainly in the form of the iodide salt ($C_5H_9IN_2S$) crystallizing in monoclinic space group $P2_1/c$. The disulfide (2,2′-disulphanylbis(1-methyl-1*H*-imidazole)), $C_8H_{10}N_4S_2$) was obtained in yellow form crystallizing in the monoclinic $C2/c$ space group.

Keywords: methimazole; impurity C hydroiodide; methimazole disulfide; crystal structures

Citation: Štefan, L.; Đilović, I.; Saftić Martinović, L.; Vianello, R.; Čikoš, A. Methimazole-Related Substances: Structural Characterization and *In Silico* Toxicity Assessment. *Crystals* **2024**, *14*, 1073. https://doi.org/10.3390/cryst14121073

Academic Editor: Alexander Y. Nazarenko

Received: 25 November 2024
Revised: 6 December 2024
Accepted: 10 December 2024
Published: 12 December 2024

1. Introduction

More than half a century has passed since methimazole (1-methyl-1,3-dihydro-1*H*-imidazole-2-thione, **1**) was introduced into clinical practice for the treatment of thyroid disorders and Graves' disease [1] in most European and Asian countries [2].

The investigation of the chemical behavior of methimazole continues to attract a great deal of attention from pharmaceutical and material scientists. This interest stems not only from its crucial role in human health, but also from its unique imidazole-thione structure.

Over the past decade, methimazole has attracted increasing attention due to its long-term use in humans and cases of misuse in veterinary medicine. This has led to a surge in publications focusing on the development and validation of analytical methods for the determination of methimazole content in various applications ranging from pharmaceutical formulations to biological samples. Recent advances have highlighted innovative methods for the detection of methimazole in complex matrices such as blood serum [3,4], meat [5], and urine [6]. For example, sensor technologies like amlodipine-gold nanoparticles and SnS_2/AuNPs have enabled rapid and selective quantification of methimazole in serum and meat samples [7], while novel chromatography and spectroscopy techniques have refined its analysis in human blood and food. This development in analytical methods is particularly significant as the European Union banned thyrostatic agents in livestock in 1981, necessitating stricter monitoring of these substances [8]. In addition to pharmaceuticals, the versatility of methimazole has also been demonstrated in other areas, such as in functionalized SERS (Surface-Enhanced Raman Scattering) optical fiber probes for ultrasensitive detection of hexavalent chromium (Cr(VI)) and as a catalyst in electroanalytical

applications [9]. The importance of understanding the chemical behavior of methimazole is reinforced by strict pharmaceutical regulations. Drug manufacturers must accurately characterize the active pharmaceutical ingredient (API)-related substituents—including impurities and degradation products—not only chemically and structurally, but also toxicologically. These regulations are driving research to develop faster, more sensitive, and robust methods for quantifying methimazole, its prodrug carbimazole, and related substances to ensure compliance with evolving standards [10].

As part of our ongoing research on methimazole-related substances [11,12] and aiming to facilitate the future identification of impurities during the methimazole production process, we decided to synthesize and systematically characterize two previously reported but never fully characterized impurities. The methimazole impurity C (1-Methyl-(2-methylthio)-1*H*-imidazole, **2a**) [13] was reported as a process impurity in the form of a liquid, while its hydroiodide salt (**2b**) is used as a precursor for the synthesis of ionic liquids [14]. Nevertheless, the available data [15,16] are inconsistent, and the crystal structure has not been published. The second impurity, methimazole disulfide (2,2′-disulphanylbis(1-methyl-1*H*-imidazole), **3**), was previously described as one of the oxidation metabolites of **1** but was never identified as one of the methimazole impurities. According to the available data, it is found in the form of a white powder [17] and polyiodide salt [18]. More recently, a yellow form of **3** has also been reported [19], but no explanation was provided for the color difference.

Complete characterization included spectroscopic, chromatographic, thermal, and computational analyses, while particular attention was given to producing the single crystals and obtaining the molecular and crystal structures. Finally, *in silico* prediction of bacterial mutagenicity was performed as recommended in International Council for Harmonisation (ICH) guidelines M7 [20].

2. Materials and Methods

2.1. General

All solvents were either distilled over suitable desiccants or purchased as puriss p.a. All reagents were used as purchased from commercial companies: CU Chemie Ueticon (Lahr, Germany) provided methimazole (**1**) 99%, Ph Eur quality (water content 0.4%); Fisher (Hampton, NH, USA) 1,2-dichloroethane (water content, 0.02%); Merck KGaA, (Darmstadt, Germany) dichloromethane and dry methanol, while Sigma (St. Louis, MO, USA) supplied acetone (water content, 0.2%). For water purification to HPLC quality grade, a Thornton 2000CRS (Mettler Toledo, Colombus, OH, USA) was used. Silica gel Kieselgel 60 F254 (Merck KGaA, Darmstadt, Germany) was used for thin layer chromatography (TLC). The spots were made visible using a UV lamp (254 nm) or I_2 vapors using 1,2-dichloroethane-MeOH 9:1 as a mobile phase.

Company EurIsotop (Saint Aubin, France) was used as source for deuterated solvents utilized in NMR spectroscopy. Bruker Avance III 600 spectrometer (Bruker, Billerica, MA, USA) with 5 mm diameter broadband probe and *z*-gradient accessory was used for NMR spectra acquisition which was performed on samples dissolved in $CDCl_3$ and DMSO-d_6 (with TMS) using standard pulse sequences at 25 °C.

Acetonitrile and ammonium acetate buffer for chromatographic analysis were both purchased from Merck KGaA (Darmstat, Germany). HPLC instrument with Agilent DAD/UV detector used gradient elution at a flow rate of 0.6 mL/min, employing mobile phase A and mobile phase B on a Zorbax C18 column. Perkin Elmer spectrophotometer was used for acquisition of the infrared spectra (IR) with ATR technique.

The thermal analysis was performed in aluminum vats with perforated lids under an inert nitrogen atmosphere with a flow rate of 55 mL/min at a heating rate of 10 °C/min on a DSC 1 instrument from Mettler Toledo (Greifensee, Switzerland). An indium metal standard was used for temperature calibration. The TGA data was acquired with a TGA/SDTA 851e system from Mettler Toledo (Greifensee, Switzerland). The sample was loaded onto a prefabricated aluminum oxide crucible and heated at a rate of 10 °C/min over the

temperature range of 25–300 °C. Nitrogen purging at 50 mL/min was maintained over the sample at 50 mL/min. The instrument was temperature-calibrated with certified $NiMn_3Al$ and nickel. The temperatures are given as initial values. All weighings were performed with a Mettler Toledo balance (Greifensee, Switzerland), which was calibrated daily according to the internal program.

Mass spectra were acquired using an Agilent 6550 iFunnel quadrupole time-of-flight mass spectrometer with dual AJS ESI source (Agilent Technologies Santa Clara, CA, USA). For positive ion mode, the capillary voltage was set to 3.5 kV, and the nozzle voltage of 1 kV. The ion source temperature was set to 200 °C, the gas flow to 14 L/min, the nebulizer pressure to 35 psi, the drying gas temperature to 350 °C, and the sheath gas flow to 11 L/min. Accurate mass measurements (High Resolution Mass Spectrometry HRMS) were obtained by ion mass correction. The references in positive ion mode were protonated purine at m/z 121.0509 protonated hexakis (1H, 1H, 3H-tetrafluoropropoxy) phosphazine, HP-921 at m/z 922.0098. The reference solution was added to the AJS ESI source to ensure that these reference compounds were included in each spectrum.

2.2. Synthesis

2.2.1. 1-Methyl-(2-methylthio)-*1H*-imidazol (**2a**)

Methimazole (**1**, 4.9 g, 43 mmol) was dissolved in a 1.5 mol/L solution of sodium carbonate (50 mL), and iodomethane (9.5 g, 67 mmol) was added for 10 min dropwise under nitrogen and stirred protected from light for 2 h at room temperature. The reaction mixture was extracted with dichloromethane (3 × 25 mL), and an organic layer dried under sodium sulfate. The solvent was evaporated in vacuo, yielding **2a** as a colorless liquid (5.2 g, 95.0%). Purity: HPLC, 100%. *Rf* = 0.59. ESI-MS: m/z [M+H$^+$] 129.0489. Molecular formula $C_5H_8N_2S$. ^{1}H NMR (DMSO-d$_6$, 600 MHz, δ/ppm): N-C$\underline{H}_3$ 3.55 (s, 3H), -N(CH$_3$)-C$\underline{H}$= 7.20 (d, 1H, *J* = 1.3 Hz), =N-C$\underline{H}$= 6.91 (d, 1H, *J* = 1.5 Hz), S-CH$_3$ 2.49 (s, 3H). ^{13}C NMR (DMSO-d$_6$, 150 MHz, δ/ppm): N-$\underline{C}$H$_3$ 32.5, C(S) 141.4, =N-$\underline{C}$H= 128.2, -N(CH$_3$)-$\underline{C}$H= 122.9, S-CH$_3$ 15.8. UV VIS λ_{max} 223 nm. IR (ATR) $\tilde{v}_{max}/cm^{-1}$: 3105, 2928, 1511, 1415, 1314, 1278, 1125, 1081, 975, 739,685.

2.2.2. 1-Methyl-(2-methylthio)-*1H*-imidazol hydroiodide (**2b**)

Methimazole (**1**, 1.0 g, 8.8 mmol) was dissolved in acetone (10 mL), and iodomethane (1.3 g, 8.8 mmol) was dropwise added to the solution, while stirring in an ice bath under nitrogen and protected from light. After two hours, the obtained crude product is filtered and washed with cold acetone yielding pure 1-methyl-(2-methylthio)-1*H*-imidazol hydroiodide (**2b**, 2.0 g, 91.0%) in the form of white crystals (2.0 g, 91.0%). Suitable single crystals were grown from acetone by slow evaporation. M.p. (DSC, onset, Figure S8) 145 °C (lit. [16] m.p. 167 °C). Purity: HPLC 99.9%. *Rf* = 0.59, ion chromatography (IC) obtained 48.2% iodine, in relation to theoretical value of 49.6%. ESI-MS: m/z [M+H$^+$] 129.0485. Molecular formula $C_5H_8N_2S$. ^{1}H NMR (DMSO-d$_6$, 600 MHz, δ/ppm): N-C$\underline{H}_3$ 3.78 (s, 3H), =N-CH= 7.76 (d, 1H, *J* = 2.0 Hz), -N(CH$_3$)-C$\underline{H}$= 7.79 (d, 1H, *J* = 2.0 Hz), S-CH$_3$ 2.71 (s, 3H). ^{13}C NMR (DMSO-d$_6$, 150 MHz, δ/ppm): N-$\underline{C}$H$_3$ 34.9, C(S) 142.2, =N-$\underline{C}$H= 120.7, -N(CH$_3$)-$\underline{C}$H= 124.9, S-CH$_3$ 16.6. UV VIS λ_{max} 226 nm. IR (ATR) $\tilde{v}_{max}/cm^{-1}$: 3076, 2387, 1928, 1775, 1681, 1580, 1426, 1359, 1283, 1127, 1093, 889.

2.2.3. 2,2′-Disulfanylbis(1-methyl-*1H*-imidazole) (**3**)

Methimazole (**1**, 2.1 g, 18.0 mmol) is dissolved in 1,2-dichloroethane (130 mL) under nitrogen with Et$_3$N (2.8 mL, 20.1 mmol). The iodine (2.3 g, 9.0 mmol) was added in portions while stirring at room temperature for 30 min. After 3 h, 100 mL of water was added to the reaction mixture, and stirring continued for another 15 min. The organic layer was washed with water, dried passing through filter paper, and evaporated in vacuo, giving the crude product, which was purified by recrystallization from EtOAc to give 2,2′-disulfanylbis(1-methyl-1*H*-imidazole) (**3**, 1.2 g, 57.6%) in the form of yellow crystals. Single crystals were grown from EtOAc by slow evaporation. M.p (DSC, onset, Figure S9) 131 °C (lit. [21] m.p.

127–128 °C, lit. [17] m.p. 138 °C). *Rf* = 0.35. ESI-MS: *m*/*z* [M+H$^+$] 227.0423. Molecular formula $C_8H_{10}N_4S_2$. ^{1}H NMR ($CDCl_3$, 600 MHz, δ/ppm): N-C<u>H</u>$_3$ 3.56 (s, 6H), =N-CH= 7.13 (d, 2H, *J* = 0.9 Hz), -N(CH$_3$)-C<u>H</u>= 7.06 (d, 2H, *J* = 0.9 Hz). ^{13}C NMR ($CDCl_3$, 150 MHz, δ/ppm): N-<u>C</u>H$_3$ 33.9, C(S) 140.2, =N-<u>C</u>H= 130.4, -N(CH$_3$)-<u>C</u>H= 124.6. UV VIS λ_{max} 300 nm. IR (ATR) $\tilde{\nu}_{max}$/cm^{-1}: 3093, 1499, 1450, 1407, 1282, 1161, 1128, 1075, 918, 790, 682.

2.3. Single-Crystal X-Ray Diffraction

Air-stable single crystals were selected to be mounted on thin glass fibers. Oxford Diffraction Xcalibur four-circle kappa geometry diffractometer with Xcalibur Sapphire 3 CCD detector using graphite monochromatic MoKα (λ = 0.71073 Å) radiation was used for acquisition of **2b** and **3** diffraction data at room temperature. CrysAlisPro software package version 1.171.39.46 [22] was used for data reduction, scaling, and absorption. The programs integrated into the WinGX version 2018.3 system [23] were used for solution, refinement, and structure analysis. Direct methods within SHELXS [24,25] were used for solving the structures. Refinement by the full-matrix least-squares methods, based on F^2 against all reflections, was performed by SHELXL [24,25], including anisotropic displacement parameters for all non-H atoms. The riding model using the AFIX routine was employed to model the hydrogen atoms bound to C and N (in **2b**). PLATON version 201118 performed an analysis of the hydrogen bonds and molecular geometry [26]. MERCURY (Version 4.1.0) [27] was used to produce the molecular graphics. Supplementary crystallographic data sets for the structures are available through the Cambridge Structural Database with deposition numbers 2,263,857 (**2b**) and 2,263,858 (**3**), respectively. Copy of this information may be obtained free of charge from the directory, CCDC, 12 Union Road, Cambridge, CB2 1EZ, UK (fax: +44-1223-336-033; e-mail: deposit@ccdc.cam.ac.uk or http://www.ccdc.cam.ac.uk, accessed on 25 November 2024).

The crystal parameters, data collection, and refinement results are summarized in Table 1.

Table 1. Essential crystallographic data for compounds **2b** and **3**.

Compound	2b	3
Chemical formula	$C_5H_9IN_2S$	$C_8H_{10}N_4S_2$
Formula weight	256.10	226.32
Crystal system	Monoclinic	Monoclinic
Space group	$P2_1/c$	$C2/c$
a/Å	8.6603(1)	12.5904(6)
b/Å	7.4999(1)	7.3959(3)
c/Å	13.7504(2)	11.2869(5)
α/°	90	90
β/°	94.826(0)	97.886(4)
γ/°	90	90
Z	4	4
F(000)	488.0	472.0
T/K	293	293
V/Å^3	889.94(2)	1041.07(8)
D_x/g cm^{-3}	1.911	1.444
2Θ range for data collection/°	9.084 to 51.988	9.102 to 56.972
Index ranges	$-10 \le h \le 10$, $-9 \le k \le 9$, $-16 \le l \le 16$	$-16 \le h \le 16$, $-9 \le k \le 9$, $-15 \le l \le 15$
Reflections collected	37,594	8880
Independent reflections	1742 [R_{int} = 0.0205, R_{sigma} = 0.0057]	1295 [R_{int} = 0.0247, R_{sigma} = 0.0151]
Data/restraints/parameters	1742/0/92	1295/0/65
S (GOF)	1.077	1.097
R [$I \ge 2\sigma(I)$]	R_1 = 0.0127, wR_2 = 0.0295	R_1 = 0.0271, wR_2 = 0.0723
R [all data]	R_1 = 0.0131, wR_2 = 0.0297	R_1 = 0.0297, wR_2 = 0.0743

2.4. Computational DFT Analysis

All molecular geometries were optimized with the DFT B3LYP/6–311+G(d,p) model, providing a good compromise between the accuracy and feasibility of the approach. The obtained electronic energies were supplemented with thermal corrections, so that all reported values correspond to free energies at room temperature and normal pressure. The effect of the solvent environment was accounted for by the SMD polarizable continuum model with all parameters for acetonitrile. UV-Vis electronic transitions were obtained by the (SMD)/CAM-B3LYP/6–311+G(d,p) single-point calculations employing the TD-DFT approach and considering 32 lowest singlet electronic excitations. All calculations were performed using the Gaussian 16 suite of programs [28].

3. Results

3.1. Synthesis

Methimazole (**1**) usually exists in a tautomeric equilibrium between 2-thione **1a** and 2-thiole **1b** (Scheme 1). It is reportedly reactive depending on the reaction conditions and the substrates employed [14]. In the context of this work, due to the exclusive use of aprotic solvents [29], the predominant form of **1** is thione tautomer, which is the reason for the formation of the thiolonium-like product **2b**.

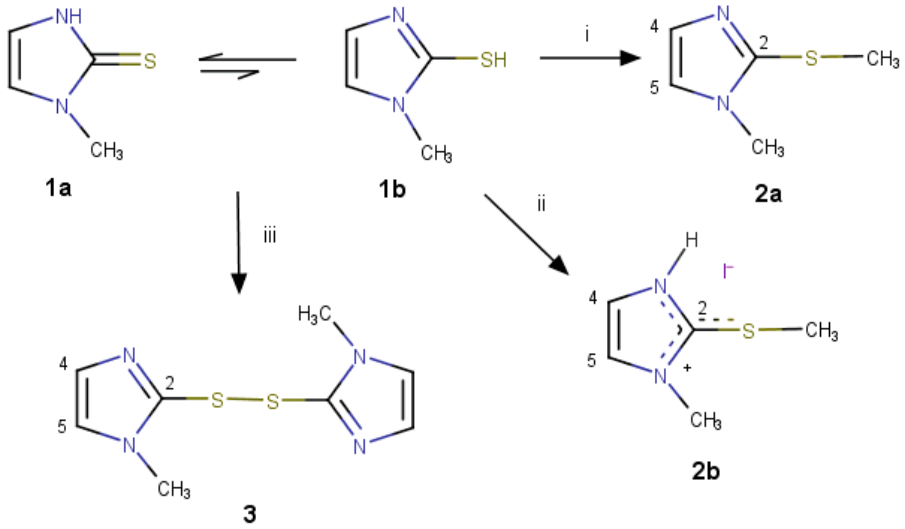

Scheme 1. Reagents and solvents: (i) CH_3I, 1 M Na_2CO_3; (ii) CH_3I, acetone; (iii) I_2, Et_3N, $(CH_2)_2Cl_2$.

Moreover, **2a** was obtained from methimazole **1** through a methylation reaction with the equimolar amount of iodomethane under basic conditions (1 M solution of sodium carbonate) at low temperatures, in an inert atmosphere, and protected from light. After 2 h, the colorless liquid separated, and the pure compound was isolated in a yield of 95.0%. However, if the same reaction is performed in acetone at room temperature for 3 h, a white crystalline product **2b** is obtained with a 91.0% yield. Its melting point is consistent with the previously reported value of 167 °C [16], while the purity determined by HPLC analysis was 99.9%.

Treating methimazole **1** with iodine in dichloroethane first results in the forming of a yellow crude material from which the pure oxidation product **3** is obtained as yellow crystals from EtOAc with 57.6% yield. The melting point of **3** was determined using DSC analysis (Figure S9) to be 131 °C (DSC onset), which differs from data previously reported (127–128 °C [21], 138 °C [17]). The attempt to obtain **3** in the colorless form by crystallization from dichloromethane, as described in the literature [17], was unsuccessful. Given that our compound differs in color and melting point from the literature, it is reasonable to assume that these two forms are different and that they might be different polymorphs. However, we could not find the powder diffractogram in the reference [17], so we could

not perform the comparison. Additionally, we have found two other publications where authors describe this compound to be yellow [19,21] which agrees well with our data.

3.2. Structure Elucidation (NMR and IR Spectroscopy, Mass Spectrometry)

The NMR analysis of ^{1}H, ^{13}C, and HSQC spectra (DMSO-d_6 at 25 °C, Figures S1–S4) revealed that all chemical shifts, signal integrals, and observed interactions are in agreement with the proposed structures for **2a**, **2b,** and **3** (Scheme 1).

The proton NMR spectrum of **2b** (Figure 1a) consists of a pair of doublets at δ_H 7.76 ppm and 7.79 ppm with a vicinal coupling constant of 2.0 Hz corresponding to the thioimidazolyl ring hydrogens. Two sharp singlets with signal integral 3 belong to hydrogens of two methyl groups: thiomethyl at δ_H 2.71 ppm and N-methyl at δ_H 3.79 ppm. The ^{13}C NMR spectrum (Figure 1c) shows the presence of methylthioimidazole carbons with signals assigned to C2 at δ_C 142.7 ppm, C4 at δ_C 121.1 ppm and C5 at δ_C 125.3 ppm. The remaining signals can be assigned to the thiomethyl carbon at δ_C 17.4 ppm, and the nitrogen methyl group at δ_C 35.6 ppm (Figure S3).

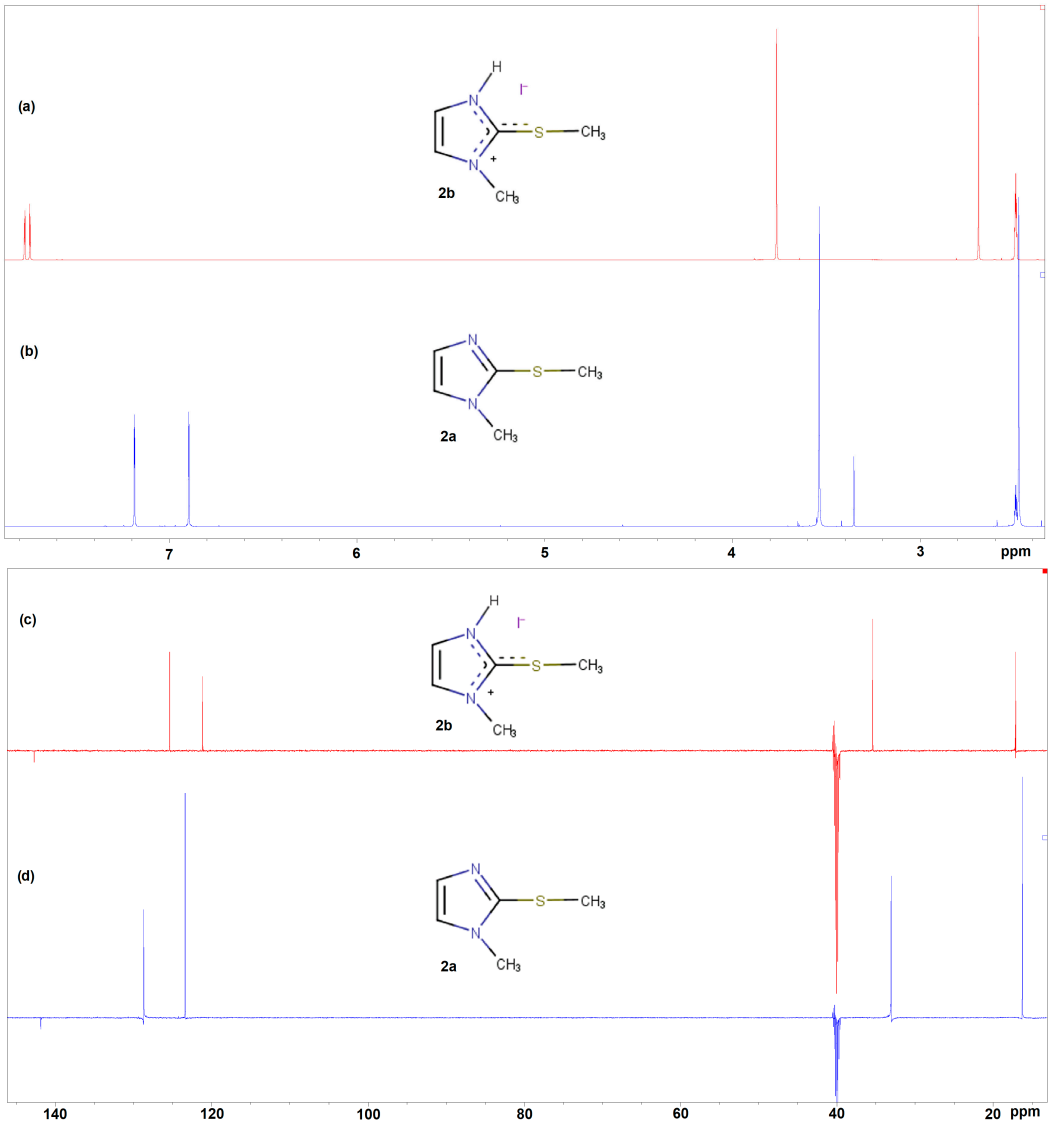

Figure 1. Comparison of ^{1}H NMR spectra for (**a**) salt **2b**, (**b**) base **2a**, and ^{13}C NMR spectra for (**c**) salt **2b**, (**d**) base **2a** at 25 °C in DMSO-d_6.

Similarly, the proton NMR spectrum of **2a** (Figure 1b) shows four signals in total: two in the aromatic region belonging to H5 (7.20 ppm) and H4 (6.91 ppm), and two in the aliphatic region belonging to two methyl groups. Expectedly, the carbon NMR spectrum (Figure 1d) showed five signals, three (141.4 ppm, 128.2 ppm, and 122.9 ppm) belonging to methylthioimidazolyl ring carbons and two (32.5 ppm and 15.8 ppm) corresponding to the two methyl carbons.

Overlay of the two proton spectra (Figure 1a,b) reveals large downfield chemical shifts of the methyl, olefinic proton, and the thiomethyl hydrogen signals of **2b** compared to non-protonated form **2a**. Likewise, a significant upfield shift of ^{13}C NMR chemical shifts was observed (Figure 1c,d) in **2b** compared to non-protonated **2a**. Such differences in ^{1}H and ^{13}C NMR chemical shifts between protonated and non-protonated imidazole moiety are well-known and reported in the literature [30]. The differences in chemical shifts result from the altered magnetic environment in **2b** due to the positive charge in the imidazole ring and the stronger H-bonding in **2b** than in **2a**.

The infrared spectrum of **2b**, when compared to **2a**, revealed new weak, broad-intensity absorption at 3115 cm^{-1}, which was assigned to the N-H stretching mode.

Both mass spectra of **2a** and **2b** were recorded in positive mode showing the most abundant ion at 129.0845 m/z, which is attributed to the base peak of **2a** corresponding to [M+H]$^{+}$ and protonated form **2b**. Furthermore, the observed fragment at 114.0427 m/z indicates the cleavage of the thiomethyl group.

The chemical structure of **3** (Scheme 1) was also elucidated using spectral analysis. The proton NMR spectrum (Figure S5) consists of a pair of doublets at δ_H 7.13 ppm and 7.06 ppm (coupling constant of 0.9 Hz) corresponding to the methylthioimidazolyl ring hydrogen atoms and a singlet at δ_H 3.56 ppm assigned to the methyl hydrogens. The ^{13}C-NMR spectrum (Figure S5) showed the presence of methylthioimidazole carbons C2 at δ 140.2 ppm, C4 at δ 130.4 ppm, and C5 at δ 124.6 ppm. The nitrogen methyl group has a resonance line at δ 34.1 ppm. In short, the signal integrals, coupling constants, proton, and carbon chemical shifts, as well as ^{1}H-^{13}C HSQC and HMBC (Figures S6 and S7, respectively) interactions, are consistent with the structure as proposed. Positive ion mode MS spectra exhibited the highest intensity ion at 227.0423 m/z, identified as the base peak of **3** and corresponding to the [M+H]$^{+}$ ion. Additionally, a fragment at 114.0249 m/z indicates cleavage of the disulfide group, resulting in the formation of two methythioimidazoyl fragments, while the fragment at 145.0432 m/z indicates cleavage of the methylthioimidazoyl group (Figure 2).

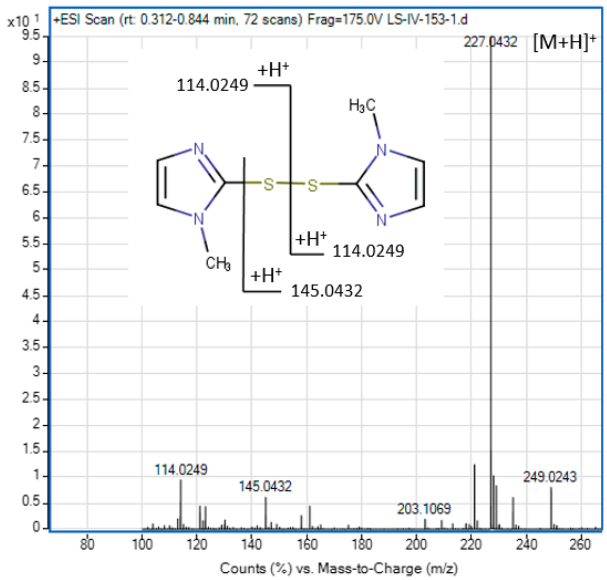

Figure 2. MS spectrum of **3**.

3.3. Single-Crystal X-Ray Diffraction

Single crystals were obtained for compounds **2b** and **3**. The resulting molecular and crystal structures are presented in Figures 3–6. Both structures' selected geometric parameters (bond lengths, and hydrogen bonding geometry) are summarized in Tables 2–4.

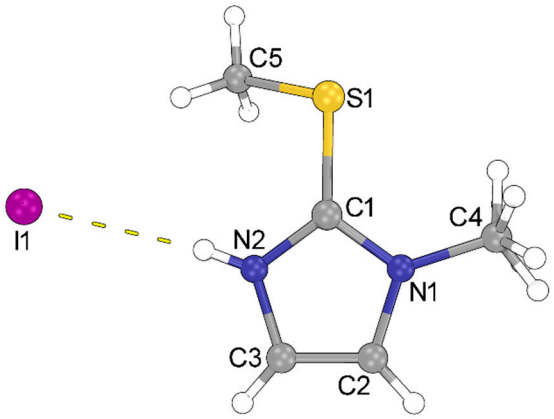

Figure 3. The asymmetric unit and atom-labeling scheme of **2b**.

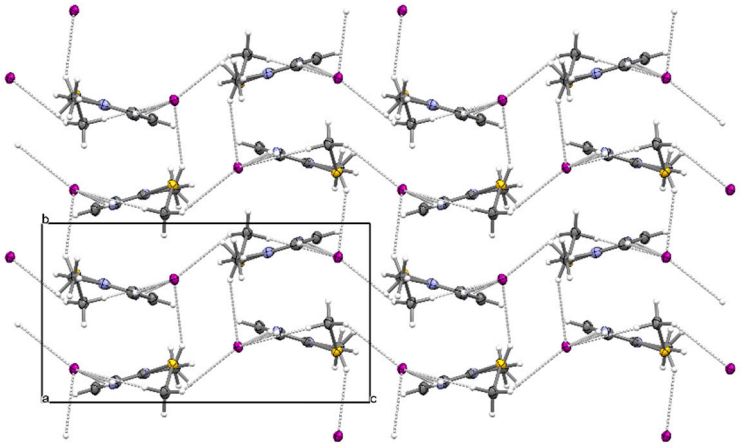

Figure 4. The crystal structure of **2b** viewed down the crystallographic *a*-axis. Hydrogen bonds are represented as arrays of white cylinders.

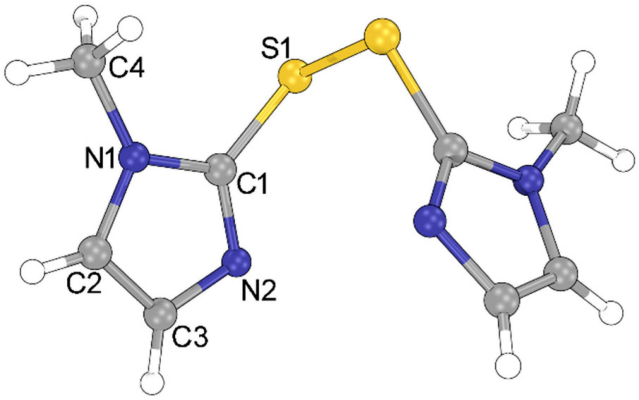

Figure 5. Molecular structure and atom-labeling scheme of **3**.

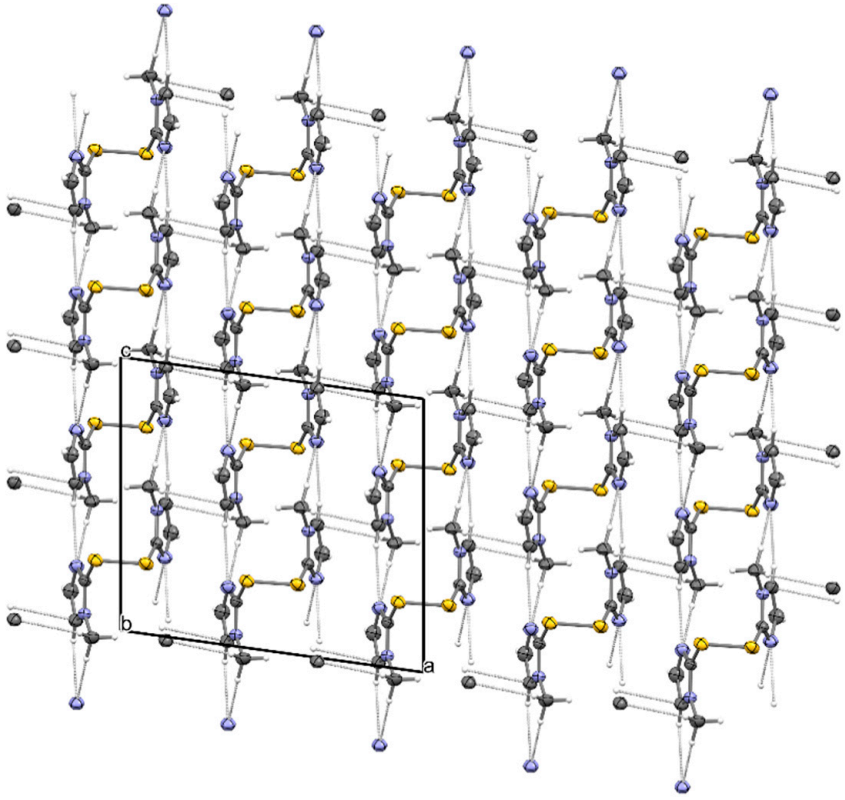

Figure 6. The crystal structure of **3** viewed down the crystallographic *c*-axis. Hydrogen bonds and C−H···π interactions (parallel to the *a*-axis) are represented as arrays of white cylinders.

Table 2. Bond lengths in **2b** and **3**.

2b/Å			**3/Å**		
C1	N2	1.334(2)	C1	N1	1.3648(17)
C1	N1	1.336(2)	C1	N2	1.3195(19)
C1	S1	1.7335(18)	C1	S1	1.7371(14)
C2	C3	1.338(3)	C3	C2	1.353(2)
C2	N1	1.380(3)	C3	N2	1.359(2)
C3	N2	1.374(2)	C2	N1	1.3610(19)
C4	N1	1.470(2)	C4	N1	1.4496(18)
C5	S1	1.8004(19)	S1	S1 ^{i}	2.0926(8)

i = −*x*, *y*, 1/2 − *z*.

Table 3. Hydrogen bonds geometry for **2b**.

D−H···A	***d*(D−H)/Å**	***d*(H···A)/Å**	***d*(D···A)/Å**	**<*d*(D−H···A)/°**
N2−H2A···I1	0.79(3)	2.74(2)	3.4992(16)	161(2)

Table 4. Hydrogen bonding geometry for **3**.

D−H···A	***d*(D−H)/Å**	***d*(H···A)/Å**	***d*(D···A)/Å**	**<*d*(D−H···A)/°**
C2−H2···N2 ^{ii}	0.930	2.620	3.4261(19)	145
C4−H2A···N2 ^{ii}	0.960	2.713	3.595 (16)	153

ii = *x*, 1−*y*, ½ + *z*.

Salt form **2b** crystallizes in the centrosymmetric monoclinic space group $P2_1/c$. The asymmetric unit consists of a positively charged methylthioimidazole moiety and an iodide ion, which are connected by a hydrogen bond of N−H···I type (graph-set notation $D^1_1(2)$, Figure 4). As expected, the heterocyclic five-membered ring is planar, with the hydrogen atom H2A on the N2 nitrogen atom. The bond lengths in the imidazole ring correspond to the usual values for delocalized systems. The C1−S1 bond is slightly shorter than the C5−S1 bond, consistent with the observation above (Table 2). The methyl sulfanyl group is rotated out of the plane of the respective heterocyclic ring. Hydrogen atoms on atoms C2, C4, and C5 also participate in weaker hydrogen bonds of C−H···I type. These hydrogen bonds connect the ions in all three directions in space.

Compound **3** crystallizes in the monoclinic $C2/c$ crystal system. Its asymmetric unit contains only one-half of the methimazole disulfide molecule. The other part is symmetry related to the first one (by a two-fold axis parallel to the crystallographic *b*-axis and perpendicular to the S1−S1 bond). The length of the disulfide S1−S1^i ($i = -x, y, 1/2 - z$) bond is 2.0926(8) Å (torsion angle C1−S1−S1^i−C1^i is 62.85(6)°). Other bonds and angles are comparable to those found in the molecules of compound **2b**. Both symmetrically related disulfide subunits (methimazole) are planar, and the angle between the planar parts is almost 33°.

According to the CSD database, the structure of the chloride salt of methimazole disulfide is also known. In the structure of that salt, both nitrogen atoms N2 are protonated, and the bond lengths are almost identical to the neutral form whose structure we describe in this paper. The molecular conformation is similar since the angle between the planar parts is close to 40°. Down the crystallographic *c*-axis, molecules are held together by hydrogen bonds of C−H···N type, where N atoms act as bifurcated hydrogen bonding acceptors (graph-set notation $R^2_1(6)$]. In addition to hydrogen bonds, there are also C−H···π interactions in the [100] direction.

3.4. Molecular Modelling

Computational DFT analysis was focused on confirming the purity of the isolated compound **3** by reproducing its UV-Vis spectra relative to parent methimazole **1** and its characterized impurity **2a** in the acetonitrile solution.

Geometry optimization identified both methimazole tautomers, yet with a significant difference in their stability. B3LYP/6–311+G (d,p) calculations reveal that **1a** is by as much as –13.0 kcal mol^{-1} lower in energy than **1b**, thus confirming the exclusive presence of the 2-thione form. This is rationalized by its relatively low N–H acidity (pK_a = 11.9) that is not matched by a generally weak basicity of the thiourea moiety (p$K_a \approx -1$), which jointly contributes to the higher 2-thione **1a** stability. When computed UV-Vis spectra are analyzed (Figure 7a), data for compound **3** reveal a dominant line with the maximum absorption at λ_{max} = 293 nm, which corresponds to a π–π^* HOMO-LUMO excitation with the computed oscillatory strength of f = 0.3437. The latter is found in excellent agreement with λ_{max} = 300 nm measured experimentally. While this notion already provides some credence to the purity of the isolated **3**, further support is offered by inspecting the data for other compounds (Figure 7b). Namely, neither of the considered systems (**1a**, **1b**, and **2a**) does not display any absorption lines close to 300 nm. In contrast, 2-thione (**1a**) and 2-thiole (**1b**) methimazole tautomers absorb at 253 nm and 205 nm, respectively, also involving π–π^* excitations with the oscillatory strength of f = 0.4166 and f = 0.3377, in the same order. Since the measured methimazole absorption occurs at λ_{max} = 265 nm, the computed values additionally confirm the exclusive presence of the 2-thione form **1a** in solution. On the other hand, the impurity **2a** is characterized by the absorption line at 211 nm (π–π^* excitation, f = 0.3671), thus being in line with λ_{max} = 223 nm measured experimentally. Taken together, all of these results support the purity of **3** when isolated as yellow crystals.

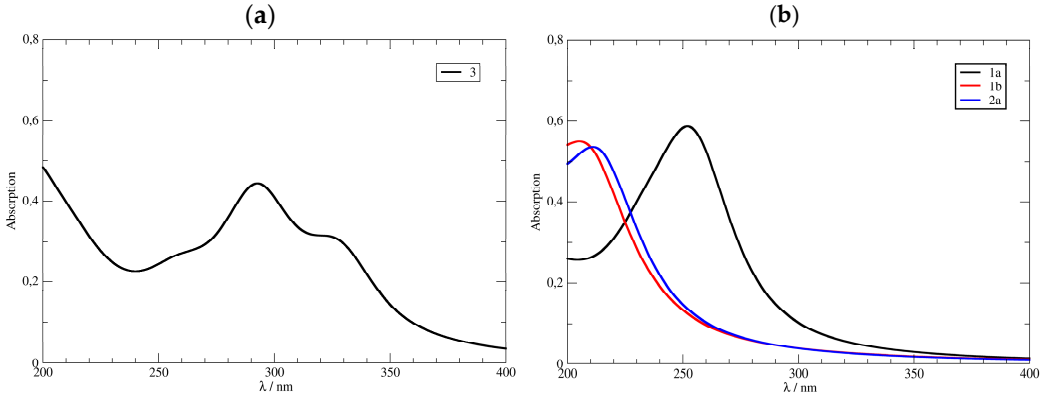

Figure 7. Computed UV-Vis spectra for different systems discussed in the text (**a**) **3** and (**b**) **1a, 1b** and **2a,** as obtained by the TD-DFT approach and the (SMD)/CAM-B3LYP/6–311+G(d,p) model in acetonitrile.

3.5. In Silico Toxicology Assessment

The *in silico* toxicology assessment is performed using at least two complement computational methods, which can predict the outcome of a bacterial mutagenicity assay. The bacterial mutagenicity (ICH M7 [20]) of **2a**, **2b,** and **3** was assessed *in silico* using (Q)SAR model within Derek version 6.3.0 [31] and Sarah version 3.3.0 [32] Nexus version 2.6.0, as well as CaseUltra version 1.9.0.8 [33] software. Two complementary (Q)SAR methods were applied: expert rule-based (Derek) and statistical-based (Sarah), neither showing any structural alerts or mutagenicity examples in the training set, which was sufficient [34–36] to conclude that none of the compounds carry mutagenic concern. CaseUltra confirmed that the result predicts all three negative compounds using the statistical model GT1_BMUT following OECD 471 guidelines. Therefore, **2a**, **2b,** and **3** were classified as ICH M7 class 5 (no structural alerts, treated as non-mutagenic impurity), and no further testing is recommended.

4. Conclusions

Although compounds **2b** and **3** have already been reported, they have never been identified as impurities that could occur during the manufacturing of methimazole. Considering methimazole's long-standing continuous use for human health, it is crucial to characterize all substances that may be present in the raw material and finished product, especially when the regulations for the pharmaceutical industry are becoming stricter every day. A complete and systematic characterization that already exists can support the quality control processes by faster identification of observed impurities in the drug material. This work summarizes the preparation of two methimazole impurities by alkylation (**2a** and **2b**) and oxidation (**3**). The compounds obtained were fully characterized, and their identifying fingerprint spectroscopic, thermal, X-ray, and computational data are included in this manuscript and accompanying Supplementary Materials. Furthermore, *in silico* mutagenicity prediction using three (Q)SAR models was performed for all compounds showing the absence of structural alerts, which classifies them as non-mutagenic ICH M7 class 5 compounds.

Supplementary Materials: The following supporting information can be downloaded at https://www.mdpi.com/article/10.3390/cryst14121073/s1, Figure S1. ^{1}H and ^{13}C spectra, structure, numbering, and full assignment of **2a** in DMSO-d_6 at 25 °C; Figure S2. ^{1}H-^{13}C HSQC spectrum of **2a** in DMSO-d_6 at 25 °C; Figure S3. ^{1}H and ^{13}C spectra, structure, numbering, and full assignment of **2b** in DMSO-d_6 at 25 °C; Figure S4. ^{1}H-^{13}C HSQC spectrum of **2b** in DMSO-d_6 at 25 °C; Figure S5. ^{1}H and ^{13}C spectra, structure, numbering, and full assignment of **3** in $CDCl_3$ at 25 °C; Figure S6. ^{1}H-^{13}C HSQC spectrum of **3** in $CDCl_3$ at 25 °C; Figure S7. ^{1}H-^{13}C HMBC spectrum of **3** in $CDCl_3$ at 25 °C; Figure S8. TGA and DSC analysis of **2** in perforated crucibles under the heating rate of

10 °C min^{-1} and N2 purge; Figure S9. DSC analysis of **3** in perforated crucibles under a heating rate of 10 °C/min and N2 purge. CCDC deposition numbers 2,263,857 (**2b**) and 2,263,858 (**3**) contain the supplementary crystallographic data for this paper. These data can be obtained free of charge via http://www.ccdc.cam.ac.uk, accessed on 25 November 2024 (or from the CCDC, 12 Union Road, Cambridge CB2 1EZ, UK; Fax: +44-1223-336033; E-mail: deposit@ccdc.cam.ac.uk).

Author Contributions: Conceptualization, L.Š. and A.Č.; investigation, L.Š., A.Č., I.Đ., L.S.M. and R.V.; data curation, L.Š., A.Č., I.Đ., L.S.M. and R.V.; writing—original draft preparation, L.Š. and A.Č.; writing—review, and editing, L.Š., A.Č., I.Đ., L.S.M. and R.V. All authors have read and agreed to the published version of the manuscript.

Funding: This research received no external funding.

Data Availability Statement: The original contributions presented in this study are included in the article/Supplementary Materials. Further inquiries can be directed to the corresponding authors.

Acknowledgments: The authors appreciate Miljenko Dumić and Dubravka Matković Čalogović for their fruitful discussions, guidance, and support.

Conflicts of Interest: The authors declare no conflicts of interest.

References

1. Taurog, A.; Dorris, M.L.; Guziec, F.S.; Uetrecht, J.P. Metabolism of ^{35} S- and ^{14} C-Labeled Propylthiouracil in a Model in Vitro System Containing Thyroid Peroxidase *. *Endocrinology* **1989**, *124*, 3030–3037. [CrossRef]
2. Cooper, D.S. Antithyroid Drugs. *N. Engl. J. Med.* **2005**, *352*, 905–917. [CrossRef]
3. Jafar, A.; Samadi, A.; Vahabzadeh, M.H. Amlodipine-Gold Nanoparticles as a New "Turn off-on" Sensor for the Sensitive Determination of Methimazole. *J. Anal. Chem.* **2020**, *75*, 402–408. [CrossRef]
4. Ito, Y.; Sakai, H.; Nagao, H.; Suzuki, R.; Odawara, M.; Minato, K. Development of a High-Performance Liquid Chromatography–Tandem Mass Spectrometric Method for the Determination of Methimazole in Human Blood Matrices. *J. Chromatogr. B* **2020**, *1144*, 122083. [CrossRef] [PubMed]
5. Zhao, X.; He, Y.; Wang, Y.; Wang, S.; Wang, J. Hollow Molecularly Imprinted Polymer Based Quartz Crystal Microbalance Sensor for Rapid Detection of Methimazole in Food Samples. *Food Chem.* **2020**, *309*, 125787. [CrossRef] [PubMed]
6. Mahmoud, A.Y.F.; Rusin, C.J.; McDermott, M.T. Gold Nanostars as a Colloidal Substrate for In-Solution SERS Measurements Using a Handheld Raman Spectrometer. *Analyst* **2020**, *145*, 1396–1407. [CrossRef] [PubMed]
7. Lai, H.; Li, G.; Zhang, Z. SnS2/AuNPs Surface-Enhanced Raman Scattering Sensor for Rapid and Selective Quantification of Methimazole in Serum and Meat Samples. *Sens. Acutators B Chem.* **2023**, *380*, 133325. [CrossRef]
8. Kritikou, A.S.; Dasenaki, M.E.; Maragou, N.C.; Kostakis, M.G.; Thomaidis, N.S. Multi-Residue Analysis of Thyreostats in Animal Muscle Tissues by Hydrophilic Interaction Liquid Chromatography Tandem Mass Spectrometry: A Thorough Chromatographic Study. *Separations* **2024**, *11*, 269. [CrossRef]
9. Long, Y.; Li, H.; Wang, W.; Yang, X.; Liu, Z. Ultrasensitive Detection of Cr(VI) Using a Novel SERS Optical Fiber Probe Modified by Dual-Functional Methimazole. *J. Alloys Compd.* **2022**, *910*, 164916. [CrossRef]
10. Kurdaikar, S.S.; Fernandes, A.; Gandhi, S.V.; Pattewar, P.; Mahajan, A.A. Spectrophotometric Determination of Carbimazole and Its Major Impurity, Degradation Product and Metabolite: Methimazole. *Opt. Spectrosc.* **2021**, *129*, 948–957. [CrossRef]
11. Štefan, L.; Matković-Čalogović, D.; Filić, D.; Dumić, M. Synthesis, Crystal Structure and Solid State Transformation of 1,2-Bis[(1-Methyl-1H-Imidazole-2-Yl)Thio]Ethane. *Crystals* **2020**, *10*, 667. [CrossRef]
12. Štefan, L.; Čikoš, A.; Vianello, R.; Đilović, I.; Matković-Čalogović, D.; Dumić, M. Chemistry of Spontaneous Alkylation of Methimazole with 1,2-Dichloroethane. *Molecules* **2021**, *26*, 7032. [CrossRef]
13. Convention on the elaboration of a European pharmacopoeia. In *European Pharmacopoeia 7.0 Thimazole*; Council of Europe: Strasbourg, France, 2010.
14. Siriwardana, A.I.; Crossley, I.R.; Torriero, A.A.J.; Burgar, I.M.; Dunlop, N.F.; Bond, A.M.; Deacon, G.B.; MacFarlane, D.R. Methimazole-Based Ionic Liquids. *J. Org. Chem.* **2008**, *73*, 4676–4679. [CrossRef] [PubMed]
15. Kister, J.; Assef, G.; Dou, J.-M.; Metzger, J. Hydrolysis of 1-Methyl-2-Methylthio-Δ2-Imidazoline. *Tetrahedron* **1976**, *32*, 1395–1398. [CrossRef]
16. Kister, J.; Assef, G.; Mille, G.; Metzger, J. Synthèse et étude du réarrangement des diazoles-1,3: Alkyl-1 alkylthio-2 (allylthio, arylthio, cycloalkylthio) imidazoles. Partie II. Réarrangement et réactions parasites. *Can. J. Chem.* **1979**, *57*, 822–830. [CrossRef]
17. Eshghi, H.; Tayyari, S.F.; Rezvani-Amin, Z.; Roohi, H. Methimazole-Disulfide as an Anti-Thyroid Drug Metabolite Catalyzed the Highly Regioselective Conversion of Epoxides to Halohydrins with Elemental Halogens. *Bull. Korean Chem. Soc.* **2008**, *29*, 51–56. [CrossRef]
18. Aragoni, M.C.; Arca, M.; Demartin, F.; Garau, A.; Isaia, F.; Lippolis, V.; Pivetta, T. A Unique Case of Polymorphism in Polyiodide Networks Resulting from the Reaction of the Drug Methimazole and I_2. *New J. Chem.* **2023**, *47*, 8122–8130. [CrossRef]

19. Vidovič, C.; Belaj, F.; Mösch-Zanetti, N.C. Soft Scorpionate Hydridotris(2-mercapto-1-methylimidazolyl) Borate) Tungsten-Oxido and -Sulfido Complexes as Acetylene Hydratase Models. *Chem. Eur. J.* **2020**, *26*, 12431–12444. [CrossRef]
20. International Council for Harmonisation of Technical Requirements for Pharmaceuticals for Human Use. *ICH Guidelines, M7 (R1): Assessment and Control of DNA Reactive (Mutagenic) Impurities in Pharmaceuticals to Limit Potential Carcinogenic Risk*; European Medicines Agency: Amsterdam, The Netherlands, 2017.
21. Arnold, H.; Vogelsang, D. Verfahren zur Herstellung von Bis-[imidazyl-(2)]-disulfid und dessen Abkoemmlingen. DE960279C, 21 March 1957.
22. *CrysAlisPro Software System*, Version 1.171.39.46; Rigaku Oxford Diffraction: Abbingdon, UK, 2018.
23. Farrugia, L.J. WinGX and It ORTEP for Windows: An Update. *J. Appl. Crystallogr.* **2012**, *45*, 849–854. [CrossRef]
24. Sheldrick, G.M. A Short History of *SHELX*. *Acta Crystallogr. A Found. Adv.* **2008**, *64*, 112–122. [CrossRef] [PubMed]
25. Sheldrick, G.M. Crystal Structure Refinement with *SHELXL*. *Acta Crystallogr. C Struct. Chem.* **2015**, *71*, 3–8. [CrossRef]
26. Spek, A.L. Structure Validation in Chemical Crystallography. *Acta Crystallogr. D Biol. Crystallogr.* **2009**, *65*, 148–155. [CrossRef]
27. Macrae, C.F.; Bruno, I.J.; Chisholm, J.A.; Edgington, P.R.; McCabe, P.; Pidcock, E.; Rodriguez-Monge, L.; Taylor, R.; Van De Streek, J.; Wood, P.A. *Mercury CSD 2.0*–New Features for the Visualization and Investigation of Crystal Structures. *J. Appl. Crystallogr.* **2008**, *41*, 466–470. [CrossRef]
28. Frisch, M.J.; Trucks, G.W.; Schlegel, H.B.; Scuseria, G.E.; Robb, M.A.; Cheeseman, J.R.; Scalmani, G.; Barone, V.; Petersson, G.A.; Nakatsuji, H.; et al. *Gaussian 16 Revision C.01*; Gaussian, Inc.: Wallingford, CT, USA, 2016.
29. Egorov, D.M.; Piterskaya, Y.L.; Dogadina, A.V. Reaction of Chloroethynylphosphonates with 1-Methyl-3H-Imidazole-2-Thiones. *Russ. J. Gen. Chem.* **2015**, *85*, 502–504. [CrossRef]
30. Pretsch, E.; Bühlmann, P.; Badertscher, M. *Structure Determination of Organic Compounds*; Springer: Berlin, Germany, 2000; ISBN 3-540-67815-8.
31. *Derek Nexus, 6.3.0*, Nexus, 2.6.0; Licensed to Syngene International (Computer Software); Lhasa Limited: Leeds, UK, 2023.
32. *Sarah Nexus, 3.3.0*, Nexus, 2.6.0; Licensed to Syngene International (Computer Software); Lhasa Limited: Leeds, UK, 2023.
33. *Case Ultra, 1.9.0.8*, Licensed to Syngene International (Computer Software); MultiCase: Mayfield Heights, OH, USA.
34. Amberg, A.; Beilke, L.; Bercu, J.; Bower, D.; Brigo, A.; Cross, K.P.; Custer, L.; Dobo, K.; Dowdy, E.; Ford, K.A.; et al. Principles and Procedures for Implementation of ICH M7 Recommended (Q)SAR Analyses. *Regul. Toxicol. Pharmacol.* **2016**, *77*, 13–24. [CrossRef] [PubMed]
35. Amberg, A.; Andaya, R.V.; Anger, L.T.; Barber, C.; Beilke, L.; Bercu, J.; Bower, D.; Brigo, A.; Cammerer, Z.; Cross, K.P.; et al. Principles and Procedures for Handling Out-of-Domain and Indeterminate Results as Part of ICH M7 Recommended (Q)SAR Analyses. *Regul. Toxicol. Pharmacol.* **2019**, *102*, 53–64. [CrossRef] [PubMed]
36. Foster, R.S.; Fowkes, A.; Cayley, A.; Thresher, A.; Werner, A.-L.D.; Barber, C.G.; Kocks, G.; Tennant, R.E.; Williams, R.V.; Kane, S.; et al. The Importance of Expert Review to Clarify Ambiguous Situations for (Q)SAR Predictions under ICH M7. *Genes. Environ.* **2020**, *42*, 27. [CrossRef] [PubMed]